THE JOURNAL OF PHYSICAL CHEMISTRY C

Article

pubs.acs.org/JPCC

Highly Luminescent Colloidal CdS Quantum Dots with Efficient Near-Infrared Electroluminescence in Light-Emitting Diodes

A. K. Bansal,[†,▽] F. Antolini,[‡,▽] S. Zhang,[†] L. Stroea,[‡] L. Ortolani,[§] M. Lanzi,[∥] E. Serra,[⊥] S. Allard,[#] U. Scherf,[#] and I. D. W. Samuel*[,†]

[†]Organic Semiconductor Centre, SUPA, School of Physics and Astronomy, University of St. Andrews, North Haugh, St. Andrews, KY16 9SS, U.K.

[‡]Photonics Micro and Nanostructures Laboratory, Fusion and Nuclear Security Department, ENEA, Via E. Fermi 45, 00044 Frascati, Rome, Italy

[§]CNR IMM Bologna Section, Via Gobetti 101, 40129 Bologna, BO, Italy

[∥]Department of Industrial Chemistry, University of Bologna, 40136 Bologna, Italy

[⊥]Materials and Chemico-Physical Processes Laboratory, Sustainable Territorial and Production Systems Department ENEA, C. R. Casaccia, Via Anguillarese 301, 00123 Roma, Italy

[#]Institut für Polymertechnologie Bergische Universität Wuppertal, Gauss-Strasse 20, 42097 Wuppertal, Germany

ABSTRACT: Quantum dots are of growing interest as emissive materials in light-emitting devices. Here first we report the formation of highly luminescent organic capped colloidal cadmium sulfide (CdS) nanoparticles having the highest photoluminescence quantum yield of 69% in solutions and 34% in neat thin films in the near-infrared range. Second, we also show efficient electroluminescence in the near-infrared from solution processed hybrid light emitting diodes (LEDs) based on such colloidal CdS quantum dots embedded in an organic semiconductor matrix forming a nanocomposite active layer. We also discuss the device structure and role of the doped active layer in efficiency improvement. With optimized active layer thickness and concentration of QDs, the device exhibits an external electroluminescence quantum efficiency of 0.62% at a peak emission wavelength of 760 nm, providing a route to solution processable flexible light sources for biosensors and medicine.

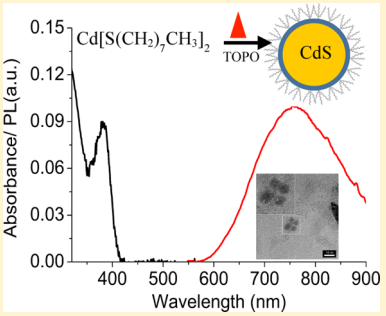

1. INTRODUCTION

Colloidal quantum dots (QDs) are an attractive choice for next generation optoelectronic devices due to their appealing physical properties of size-tunable band gaps, good photostability, photoluminescence efficiency, and compatibility with solution-processing methods.[1−3] Among reported applications, QDs have been actively investigated for light-emitting diodes (LEDs),[4] photodetectors,[5] solar cells,[6] and biolabeling[7] as well as down-converters in backlit displays.[8] Recently visible quantum dot based OLEDs using CdSe/CdS core−shell nanocrystals were reported with record external quantum efficiency (EQE) of 18% and peak emission at 620 nm.[9] In order to explore their potential for biomedical and sensing applications, efforts have been made to extend the optical response of colloidal quantum dots from the visible to the near-infrared (NIR) using nanocrystals based on, for example, CdSe, CdTe, and PbS.[10,11] However, the efficiency of solution processed OLEDs in NIR emission is very low[12] and there is a large gap in reported performance between the impressive visible results and NIR devices. Organic molecule/nanocrystal hybrid devices were reported recently having core−shell nanocrystals in the NIR range with EQE up to 0.4% with peak emission at 884 nm and maximum 2% with peak emission at 1054 nm.[13] Colloidal quantum dots capped by organic ligands are simple to make and widely studied but also have low efficiency in the infrared. For example PbS capped with oleic acid, the electroluminescence peaks at 1250 nm and has an efficiency of just 1.1%.[14] EQEs of these devices are limited by the photoluminescence quantum yield (PLQY) of QDs in a thin film which is less than 10%, so if QDs with higher PLQY can be developed, EQEs should proportionately increase. Still to our knowledge there is no systematic report available on the development of efficient colloidal QDs based OLED emitting in the wavelength range 700−900 nm, which is known as the therapeutic window[15] for biological applications.

In this article we report an advance in PLQY and external EQE for NIR emission based on ligand-capped CdS quantum dots. We explore ligand-capped materials for two reasons. First, they are simple to prepare, and second, we found surprisingly high emission in the NIR region of the spectrum. In particular we have exploited the formation of efficient surface trap emission in tri-*n*-octylphosphine oxide (TOPO) capped CdS QDs with PLQY up to 69% in solutions and surprisingly show that it can lead to efficient emission for the fabrication of a

Received: September 18, 2015
Revised: December 13, 2015
Published: December 14, 2015

DOI: 10.1021/acs.jpcc.5b09109
J. Phys. Chem. C 2016, 120, 1871−1880

hybrid LED. In this article the formation of the colloidal CdS QDs was studied by absorption and photoluminescence measurements and additional understanding of the QD growth and quality was achieved by high-resolution transmission electron microscopy (TEM) techniques. The effect of surface ligands on QDs was studied to understand their emissive properties. Furthermore, we fabricated hybrid LEDs and compared two device architectures: one contains a monolayer of QDs; the other places the QDs in an organic host matrix. The resulting electroluminescence was due either to direct carrier injection into QDs followed by exciton formation and recombination on the QD or to exciton formation in organic films followed energy transfer to the QDs.[7] Our results show that for ligand-capped QDs higher efficiency is obtained for devices using an organic host matrix than for those using a monolayer of QDs.

2. MATERIALS AND METHODS

2.1. Synthesis of Cadmium Bis-octanthiol Precursor. An amount of 1.83 g of $CdCl_2$ (10 mmol) has been dissolved in 100 mL of water/EtOH 1:1 (v:v), and then a volume of NH_4OH 35% is added until a white suspension disappears (approximately 10−11 mL of ammonium hydroxide solution) and the solution becomes clear again. In the $CdCl_2$ solution a volume of 3.47 mL of octanthiol (20 mmol) is added drop by drop. A white precipitate is immediately formed, and the solution is then left to stir for 2 h at room temperature. The precipitate is centrifuged at 4000 rpm for 10 min, and then the powder is resuspended in water/EtOH 1:1 (v:v) again and centrifuged at 4000 rpm for 10 min. This washing procedure is repeated twice. The white powder is finally dried overnight in air (yield 85%). *Elem. analysis*: Calculated for $C_{16}H_{34}CdS_2$: Cd, 27.9%; C, 47.7%; H, 8.5%; S, 15.9%. Found: Cd, 24.92%; C, 47.95%; H, 8.76%; S, 15.98%. FTIR (KBr, cm^{-1}): 2955 (antisymmetric stretching $-CH_3$); 2921 (antisymmetric str $-CH_2-$); 2872 (symmetric str $-CH_3$); 2849 (symmetric str $-CH_2-$); 1466 ($-CH_2-$ deformation); 1378 ($-CH_3$ deformation); 722 ($-CH_2-$ rocking); 647 (C−H deformation).

$$CdCl_2 + 2CH_3(CH_2)_7SH \xrightarrow[rt]{EtOH/H_2O} Cd[S(CH_2)_7CH_3]_2 + 2H^+ + 2Cl^- \quad (1)$$

The NMR analysis was carried out in the solid state because the compound is insoluble. ^{13}C (^1H) CPMAS solid state spectrum: MAS speed 25 kHz, T = ambient. The expected resonances are 8, but the signals seem to be the double. This phenomenon could be ascribed to the presence of two different phases (crystalline and amorphous) on the powder. Starting from the methyl group (C8) to the methylene $-CH_2-$ bound to the S atom the chemical shifts are 15.07 ppm (C8 $-CH_3$), 24.52 ppm (C7 $-CH_2-$), 28.25 ppm (C6 $-CH_2-$), 30.51 ppm (C5 $-CH_2-$), 32.75 ppm (C4 $-CH_2-$), 34.92 ppm (C3 $-CH_2-$), 39.07 ppm (C2 $-CH_2-$), 41.62 ppm (C1 $-CH_2-$).

2.2. Time Course of CdS Formation. A three-neck flask of 50 mL has been loaded with 24 g of TOPO. The powder has been heated at 120° under vacuum (50 mbar) and stirring for 30 min, then the solvent has been brought at 220 °C under nitrogen for additional 30 min. A solution of trioctylphosphine (TOP)/cadmium bis-octanthiol has been prepared by resuspending 480 mg of Cd bis-octanthiol in 15.4 mL of TOP (the mole ratio between TOP/precursor is set at 29) under nitrogen and stirring for 1 h. The TOP/precursor solution is injected into the hot TOPO. After the injection the temperature drops down to 180 °C, then the heater is switched to maximum temperature and within 5−10 min the temperature is stabilized to 220 °C. Starting from this moment a volume of 5 mL of the reaction mix has been taken time by time to study the time course of the CdS QDs formation. A volume of 5 mL has been kept at 30, 60, 75, 90, 120, 150, 180, and 240 min, and the reaction was stopped by cooling the solution at room temperature.

The solution is then poured in 45 mL of acetone and kept at −20 °C for 20 min to help the precipitation of the QDs. The QDs were recovered by centrifuging the suspension at 4000 rpm for 20 min. The pellet is dissolved in 200 μL of chloroform and distributed into two Eppendorfs. A volume of 1.2 mL of acetone has been added to each Eppendorf to further precipitate and purify the QDs. The solution is then centrifuged at 14,000 rpm for 10 min. The dissolution/precipitation step has been repeated twice. Finally the pellet is redissolved in 0.5 mL of chloroform for the final optical and structural characterization.

2.3. Effect of TOP, DPP, and OA on CdS QDs Optical Properties. In a typical reaction an amount of 20.5 mg of Cd bis-octanthiol (0.05 mmol) was loaded in a Pyrex tube. A volume of 3 mL of octadecene (ODE) (previously degassed under vacuum, 50 mbar, at 120 °C for 30 min, then under N_2 for 30 min) or TOPO (previously degassed under vacuum, 50 mbar, at 120 °C for 30 min, then under N_2 for 30 min) is added to the test tube. To this solution an amount of 1.5 or 0.5 mmol, or 0.15 or 0.05 mmol of TOP, diphenylphosphine (DPP), or oleic acid (OA) is rapidly injected and the reaction was carried out under N_2. In the case of ODE (or TOPO) combined with both OA and DPP the content of OA has been kept constant at 0.05 mmol (ratio OA to precursor is 1) while the DPP is varied from 0.05 to 1.5 mmol (ratio DPP/precursor of 1, 3, 10, 30). The test tube was immediately put in a stirrer set at the desired temperature (220 °C) for 60 min. During the first 5 min the temperature within the Pyrex tube drops to 210 °C, then reaches once again the selected value.

The reaction was stopped by cooling the tube to room temperature using water, and then the mixture was poured into 40 mL of acetone. The QDs grown in TOPO were purified as reported above. The QDs grown in ODE were purified following the same protocol with minor modifications. The reaction mix was stopped in cold water and the solution poured into 40 mL of acetone as described above. Then a volume of 2−5 mL of acetonitrile was added as soon as the solution became cloudy. The solution was then centrifuged at 4000 rpm for 20 min. The precipitate was redissolved with 0.2−0.4 mL of chloroform and was transferred to Eppendorfs. For a chloroform volume of 0.2 mL, 1.2 mL of acetone/acetonitrile 1:1 (v/v) was added and the solution was then centrifuged at 14,000 rpm for 10 min. The precipitate was washed once again with 1.2 mL of acetone/acetonitrile 1:1 (v/v), and then the precipitate was resuspended in 0.5 mL of cloroform.

2.4. Optical Characterization of the Samples. The solutions were analyzed by both UV−vis and PL spectroscopy. The UV−vis spectra were recorded by dissolving a volume (5−50 μL) in 3 mL of chloroform in such a way that the absorbance at 350 nm was about 0.1. The absorption cross section (σ_{QDs}, cm^2) has been calculated from the absorbance spectrum using the following formula:[16]

DOI: 10.1021/acs.jpcc.5b09109
J. Phys. Chem. C 2016, 120, 1871−1880

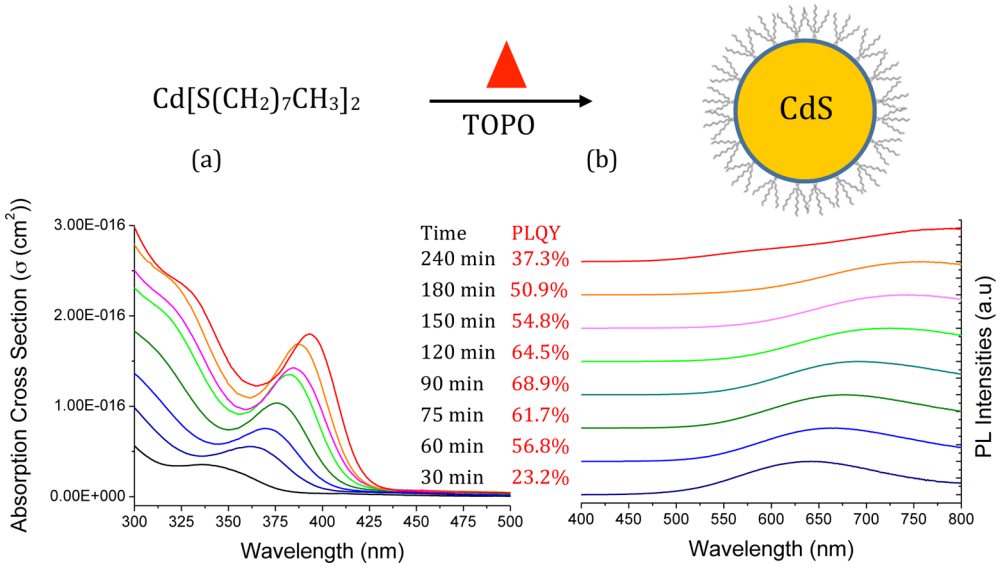

Figure 1. (a) Absorption cross section spectra and (b) photoluminescence spectra of the TOPO capped cadmium sulfide QDs in solutions at various times during synthesis. The sample was excited at 360 nm. The spectra in (b) are offset vertically to improve the readability of the curves. The figure also show the chemical formula of the precursors and representation of TOPO capped QDs after thermolysis.

$$\sigma_{QDs} = \frac{2.303(OD)}{N_{QDs} l}$$

where OD is the optical density taken from the absorption spectrum of the QDs in solution, l is the cuvette path (1 cm), and N_{QDs} is the number of QDs per cm^3. The value of N is determined from the concentration (mol/L) calculated as reported by Yu et al.:[17]

$$N_{QDs} = \frac{\text{Conc}(6.02 \times 10^{23})}{10^3}$$

where 6.02×10^{23} is the Avogadro number and 10^3 is a conversion factor from dm^3 to cm^3.

The same solution was then used to record the PL spectra and to determine the PLQY with excitation at 360 nm, which was measured using a Hamamatsu integrating sphere[18] measurement system. The PL spectra were recorded in the region between 400 and 800 nm, with an emission bandwidth of 1.6 nm and excitation of the sample at 350 nm with an excitation bandwidth of 1.8 nm, dwell time 0.6 s, and step 1 nm (FSP920 Edinburgh Instruments). The PL spectrum was then corrected for the system response.

2.5. CdS QDs Size Determination and Size Distribution. The fwhm has been determined by using the Origin program converting the x axis of the absorption spectrum (wavelength vs Abs) in a new graph where the wavelength has been changed in QDs size using the Yu et al.[17] equation (particle size vs Abs). Then the absorption peak of the CdS has been fitted with the Gaussian curve by obtaining the fwhm of the particle size. The particle size distribution, σ, is calculated from the fwhm values by using the following relationship valid for the Gaussian distribution:

$$\sigma = \frac{\text{fwhm}}{2.355}$$

The curve fitting of the particle size and fwhm have been obtained with the asymptotic equation $y = a - bc^x$. In the case of size the fitting parameters are $a = 3.147 \pm 0.037$, $b = 2.306 \pm 0.106$, and $c = 0.983 \pm 0.001$ with a R^2 of 0.993. In the case of fwhm the fitting parameters are $a = 1.210 \pm 0.043$, $b = 0.263 \pm 0.123$, and $c = 0.983 \pm 0.014$ with a R^2 of 0.519. The statistical treatment of the PLQY and photoluminescence max (average values and standard deviations shown in Figures 3 and 4) has been carried out on three different samples for each ligand/precursor ratio.

2.6. Thin Film and Devices Fabrication. For optical spectroscopy, thin films of QDs were spin-coated on fused silica substrates. The absorption spectra were measured using a Varian UV spectrophotometer, and photoluminescence spectra were measured with a FLS980 Edinburgh Instruments fluorimeter. For devices, ITO-coated soda lime glass substrates were cleaned by ultrasound in acetone and 2-propanol, followed by an oxygen plasma treatment. A 40 nm thick poly(3,4-ethylenedioxythiophene):poly(styrenesulfonate) (PEDOT:PSS) was spin-coated on the ITO and baked on a hot plate at 120 °C for 10 min. A hole-transport layer of 35 nm thick poly(*N*-vinylcarbazole) (PVK) was spin-coated on the PEDOT:PSS layer and baked at 80 °C for 2 h in a nitrogen glovebox. An emissive layer of either QDs alone or QDs blended with (4,4′-*N*,*N*′-dicarbazole)biphenyl (CBP) and 4-diphenylphosphoryldibenzofuran (o-DBFPPO) was spin-coated on top of the PVK layer. An electron-transport layer of 60 nm thick bis-4,6-(3,5-di-3-pyridylphenyl)-2-methylpyrimidine (B3PyMPM) was deposited through a shadow mask. A cathode of Ca/Al (20 nm/100 nm) was then deposited on the B3PyMPM layer in the same vacuum system. After the evaporation, the devices were encapsulated with optical curing adhesive (Norland NOA68) and glass coverslips in the glovebox. The device has an active area of 2×1.5 mm^2. The current−voltage−light output characteristics were measured using a Keithley source measure unit with a calibrated silicon photodiode. The EL spectra were measured using a charge coupled device spectrograph.

3. RESULTS AND DISCUSSION

3.1. Photophysical and Structural Characterization of Quantum Dots. The synthesis of the single source precursor Cd bis-octanethiol ($Cd[S(CH_2)_7CH_3]_2$) has been carried out

DOI: 10.1021/acs.jpcc.5b09109
J. Phys. Chem. C 2016, 120, 1871−1880

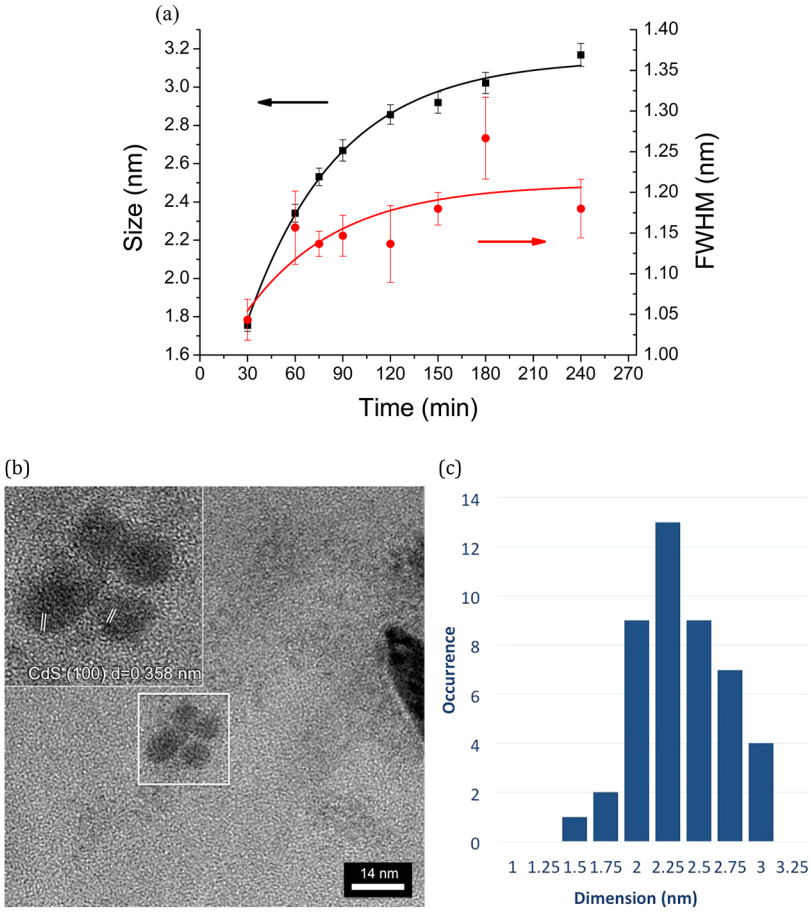

Figure 2. (a) Size (black square, experimental values; black line, asymptotic fitting) and fwhm (red dot, experimental values; red line, asymptotic fitting) trend of the CdS growth from cadmium octanthiol at 220 °C. (b) TEM characterization of CdS nanoparticles, appearing with darker contrast on the amorphous carbon film of the TEM grid. (Inset) High-resolution TEM image of four CdS clusters, showing lattice fringes from CdS (100) crystal planes. (c) Histogram for the calculation of the mean size and particle size distribution determined on 45 QDs.

using the protocol proposed by Rees et al.[19] with minor modifications as shown in reaction 1 in the experimental section. A schematic representation of colloidal TOPO capped CdS QDs after the thermolysis of the cadmium bis-octanethiolate precursor performed in the presence of a coordinating solvent TOPO is shown in Figure 1. The growth of the QDs was carried out in a reaction flask at elevated temperature at 220−270 °C, and the time course growth dynamics of the QDs were monitored at different reaction times. Figure 1 shows absorbance and photoluminescence of such TOPO capped QDs at various reaction times. The absorption spectra show a well-defined shift in the band edge absorption at various reaction temperatures, and all QDs absorb below 420 nm. For example, as shown in Figure 1a the band edge absorbance of the QDs moves from 340 nm at 30 min reaction time to 380 nm after a reaction time of 240 min at a temperature of 220 °C. These particular QDs did not show any band edge emission when excited in solutions at 350 nm but emitted at longer wavelength, a broad emission with peak up to 790 nm in the near-infrared (NIR) as shown in Figure 1b. The PL maxima shift toward red as a function of baking time within the interval 640−790 nm shows the dependence of the PL properties on the QDs size.

Surprisingly these CdS QDs are highly emissive, and values of PLQY obtained are shown in Figure 1. The time course of the PLQY shows a rapid increase to a maximum of 68.9% during the first 90 min and then a decrease to 37% upon further heating. The high PLQY is surprising considering that QDs are obtained with the use of an organic ligands system TOP/TOPO. In literature CdS QDs have been reported to emit at these longer wavelengths if the surface of the nanocrystals is not passivated completely, but nonradiative recombination due to the associated defect states leads to very weak emission with less than 1% PLQY.[20] High PLQY has been reported earlier in CdTe QDs using thiol ligands[21] where authors suggest that the PLQY is a function of the steric hindrance of the ligand.

Figure 2a shows the size distribution of the CdS QDs determined by optical spectroscopy as a function of the annealing time together with the full width at half-maximum (fwhm). The size of the CdS QDs was determined using the equation proposed by Yu et al.[17] In the initial period (30−90 min), there is a rapid enhancement of the size of CdS QDs followed by a slower growth during 120−240 min as soon as the precursor decomposed. This trend correlates with the classical La Mer model of nucleation and growth followed by the Ostwald ripening where the larger particles are formed at the expense of the smaller ones.[22,23] The fwhm, which is a direct indicator of the particle size distribution, increases with the time of annealing from 1.04 ± 0.02 to 1.18 ± 0.04. This size defocusing suggests the role of the Ostwald ripening mechanism during the growth of particles.[23] Figure 2b shows the transmission electron microscopy (TEM) image of CdS

DOI: 10.1021/acs.jpcc.5b09109
J. Phys. Chem. C 2016, 120, 1871−1880

QDs, showing the maximum PLQY, deposited on the amorphous carbon film of a standard TEM carbon grid. The smaller nanoparticles with diameter below 3 nm are homogeneously distributed over the TEM grid, appearing with dark contrast over the amorphous film, and the bigger clusters clearly show crystal structure. In the inset of Figure 2b, displaying a magnified view of the area highlighted by the white rectangle, lattice fringes corresponding to CdS (100) crystal planes are highlighted. TEM analysis of the dimension of the CdS clusters (histogram shown in Figure 2c) reveals that the CdS QDs mean size is 2.2 nm and the particle size distribution is 0.4 nm. The mean size and the particle size distribution obtained from optical analysis for the same sample (220 °C, 60 min of annealing) are respectively 2.3 and 0.5 nm, indicating the good agreement between the structural and optical analyses.

3.2. Effect of Ligands on Photophysical Properties of Quantum Dots. In order to understand the formation of such highly emissive QDs, we carried out a detailed photophysical study of various ligands on the QDs. It is well-known that the optical properties of the QDs and their PL quantum yield are strictly correlated with surface ligands. The role of the ligands is to modulate the surface defects of QDs. The dangling bonds on the exposed surfaces of the QDs can be passivated by the ligands so that deep trap emission states can be consequently modulated.[24] In metal chalcogenide QDs, chalcogen filled states and metal derived empty states can lead to mid gap states which work as an ideal passivation system for both of them.[25] The effect of the ligands on photophysical properties and in particular on PLQY is reported for several types of II−VI QDs and in particular for CdTe[21,26,27] and CdSe.[28−30]

In the system reported here the CdS QDs were synthesized from a single source precursor (SSP) with a solvothermal synthesis process in the presence of TOP and TOPO which act as ligands and a good solvent for precursor. As the photophysical properties of the QDs depend upon the growth conditions and surface ligands, the combined effect of photoluminescence emission at longer wavelength coupled with a high PLQY has been investigated by changing the solvent and the ligand type in the reaction synthesis. The synthesis of the CdS was carried out on TOPO, a coordinating solvent and ODE, a noncoordinating solvent using TOP, diphenylphosphine (DPP), and oleic acid (OA) in the reaction media and changing their ratio with respect to the CdS single source precursor.

Figure 3 shows the effect of TOP, DPP, and OA in ODE, in both the PLQY and wavelength shift of the photoluminescence maxima (PL max) of the CdS QDs. As shown in Figure 3a, a relatively high PLQY (34.7 ± 3.1%) is observed only when OA and DPP are used together with ODE. Neither oleic acid alone nor TOP or DPP is enough to stimulate the PLQY of ODE which decreases further as the amount of OA is increased. On the other side a red shift of the PL max is obtained only when the OA is present in the reaction mixture either alone or in combination with DPP (between 600 and 800 nm). In the case of ODE/OA reaction mixture, this red shift is dependent on the amount of OA (Figure 3b), while in the case of ODE/OA/DPP reaction the wavelength of PL maximum does not change because the concentration of OA remained constant (the OA/precursor ratio is equal to 1, and the DPP concentration is enhanced from 0.05 to 1.5 mmol). These interesting results show that the presence of OA in ODE solvent red-shifts the PL max while a relatively high PLQY is obtained only when OA and DPP are combined in the reaction mix.

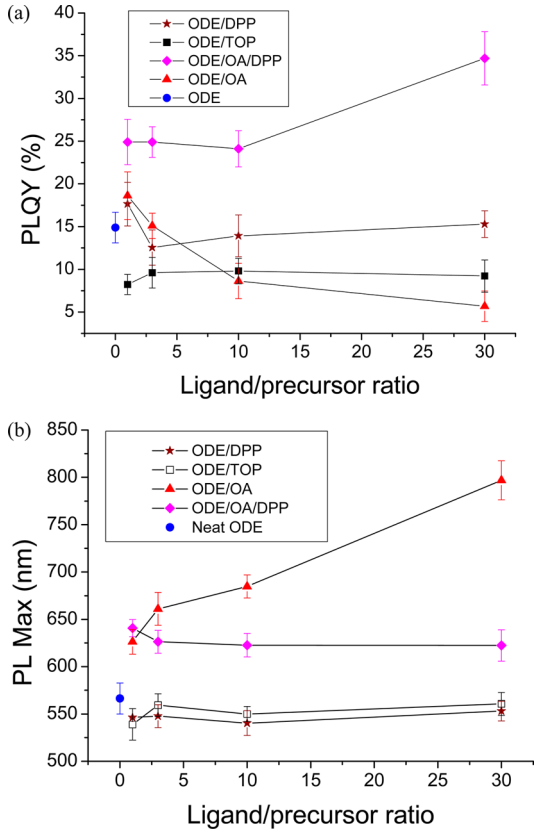

Figure 3. (a) PLQY of the CdS QDs grown in ODE as a function of ligands/precursor molar ratio. (b) Photoluminescence maxima (PL max) of the CdS QDs grown in ODE as a function of ligands/precursor molar ratio. In both cases the ligands are TOP, DPP, and OA. When OA and DPP are used in combination, the amount of OA is kept constant with respect to precursor (0.05 mmol, ratio with respect to precursor equal to 1).

The effects of the ligands on the PLQY and PL max of the CdS QDs grown in TOPO are shown in Figure 4. In this system the PLQY (Figure 4a) is low in neat TOPO and in a mixture of TOPO/OA. On the contrary when TOPO is coupled with a high amount of TOP (ratio more than 3) or DPP or OA/DPP, the quantum yield abruptly increases to 69%. The dependence of the PLQY on TOP concentration is probably due to the presence of the more reactive dioctylphosphine (DOP) that is present as an impurity in TOP.[31] Indeed it has been recently highlighted that DOP is the key reagent affecting the optimal growth of the QDs.[32] This effect has not been observed for DPP, as the PLQY is practically high and constant for most of the interval as shown in Figure 4a, because it is a more reactive reagent[33] than TOP, so there is no requirement to add it in large excess. The effect of these ligands on the PL max red shift is shown in Figure 4b. In this case all the samples show a PL max shifted toward the region between 650 and 725 nm except for neat TOPO and TOPO/TOP with low concentration of TOP (PL max of 570 and 553 nm, respectively). These results confirm the role of OA concentration shifting the PL max toward red when coupled with TOPO.

All these lines of evidence can be understood by considering the role of OA and TOPO as cadmium ligands[25,34] and TOP/DPP as sulfur ligands.[24,33,35] Tables 1 and 2 resume clearly the role of the ligands for enhanced PLQY and red shift of PL max.

DOI: 10.1021/acs.jpcc.5b09109
J. Phys. Chem. C 2016, 120, 1871−1880

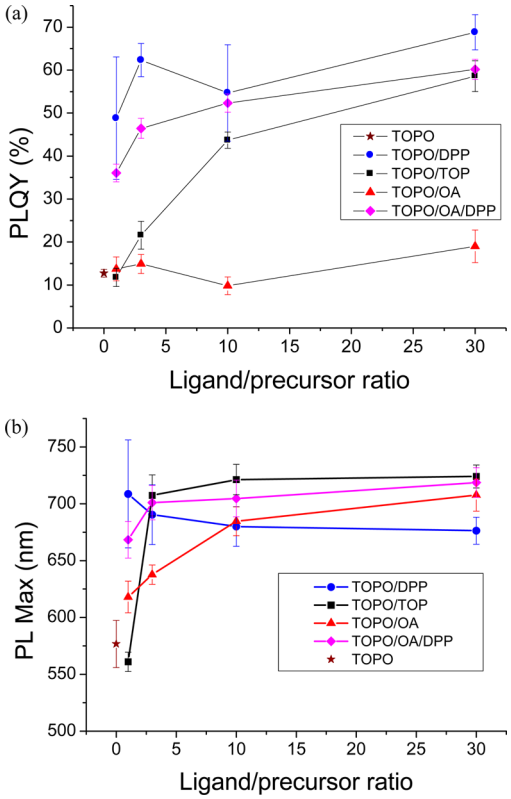

Figure 4. (a) PLQY of the CdS QDs grown in TOPO as a function of ligands/precursor molar ratio. (b) Photoluminescence maxima (PL max) of the CdS QDs grown in TOPO as a function of ligands/precursor molar ratio. In both cases the ligands are TOP, DPP, and OA. When OA and DPP are used in combination, the amount of OA is kept constant (0.05 mmol) with respect to precursor (ratio equal to 1).

Table 1[a]

	ODE Solvent	
ligand	PLQY (%)[a]	PL max (nm)[a]
	14.9 ± 1.8	566 ± 16
TOP	9.2 ± 1.9	560 ± 12
DPP	15.3 ± 1.5	553 ± 10
OA	5.7 ± 1.8	797 ± 21
OA/DPP[b]	34.7 ± 3.1	622 ± 17

[a]These are the values obtained with the ligand concentration of 1.5 mmol (ratio 30 with respect to the single source precursor). [b]OA, 0.05 mmol constant.

Table 2[a]

	TOPO Solvent	
ligand	PLQY (%)[a]	PL max (nm)[a]
	12.7 ± 0.9	577 ± 21
TOP	58.6 ± 3.6	724 ± 10
DPP	68.7 ± 3.7	676 ± 12
OA	19.0 ± 3.8	708 ± 14
OA/DPP[b]	60.2 ± 2.4	719 ± 13

[a]These are the values obtained with the ligand concentration of 1.5 mmol (ratio 30 with respect to the single source precursor). [b]OA, 0.05 mmol constant.

From Table 1 it is clear that OA is the key reagent for the red shift of PL max because the red shift is observed only when the OA is present. However, this ligand alone is not enough to enhance the PLQY. On the other side the presence of TOP or DPP alone does not stimulate the PLQY or red shift of PL max. When only both OA and DPP are present, the PLQY is enhanced and the PL is red-shifted. At the molecular level this means that the coordination of cadmium on the QDs surface is due to OA which shifts the PL emission but the defects on the sulfur dangling bonds cause the loss of energy. High PLQY is achieved only when OA is coupled with DPP, a sulfur ligand, which reduced many of the defects both on the Cd and S atoms.

Table 2 shows the same scheme for TOPO solvent. As expected, the neat TOPO is not able to promote a high PLQY because the sulfur defects are not reduced. Interestingly neat TOPO does not display a red shift of the PL because it is a cadmium ligand. The red shift of PL is observed only in the presence of OA. This indicates that OA is a stronger ligand for cadmium than for TOPO and only its presence can stimulate this red shift. Obviously the PLQY in both cases is low because the sulfur atoms on the surface are unbounded. As soon as the TOPO/OA (or TOPO) is treated together with DPP (or TOP), the high PLQY is restored. Interestingly OA seems not crucial when TOPO is present in combination with TOP or DPP to obtain high PLQY coupled with red shift of PL. This could be due to the presence of impurities in TOPO that interact with DPP and stimulate the shell formation over the growing QDs. Indeed it has been already shown that TOPO impurities such as di-*n*-octylphospine oxide (DOPO) and di-*n*-octylphospinic acid (DOPA)[31,32] can modulate the growing QDs. These results suggest that the variability of optical properties of CdS QDs upon the TOPO impurities is per se a critical point in QDs growth. However, the addition of OA to the reaction mix is beneficial to obtain QDs with standardized optical properties.

The ODE, ODE/DPP, TOPO, and TOPO/DPP were also analyzed with TEM in order to verify if the composition and crystalline structure of the samples are also responsible for the different optical properties of the QDs. Indeed it is reported that cubic (zinc blend) and hexagonal (wurzite) phases have different PL emission properties.[29] Figure 5 summarizes TEM characterization. Figure 5a–c refers to TOPO samples, Figure 5d–f to the TOPO/DPP, Figure 5g–i to the ODE samples, and Figure 5j–l to the ODE/DPP. The analysis combining imaging, electron diffraction, and elemental analysis with X-ray spectroscopy (EDS) reveals that the QDs present in all cases have the cubic structure indicating that the crystalline structure is not responsible for the optical properties.

The behavior of QDs in solid state samples was also studied where thin films of QDs were prepared by spin-coating the solutions at 1200 rpm on quartz substrates. The photoluminescence quantum yield of neat films of our QDs was measured using an integrating sphere. The nanocrystals show PL quantum yield up to 34% which to our knowledge is the highest value from colloidal QDs passivated by organic molecules in the NIR range. Such high PLQY values stimulate us to fabricate the devices using these QDs, and the results are discussed in next section.

3.3. Devices Characterization. The device architecture with corresponding energy levels of various layers is shown in Figure 6, in which the electrode work functions and the HOMO/LUMO energies for PEDOT, PVK, CdS QDs,[36] o-DBFPPO, and B3PyMPM are taken from the literature.[37,38] Three different sets of devices were fabricated. In set 1, the

DOI: 10.1021/acs.jpcc.5b09109
J. Phys. Chem. C 2016, 120, 1871–1880

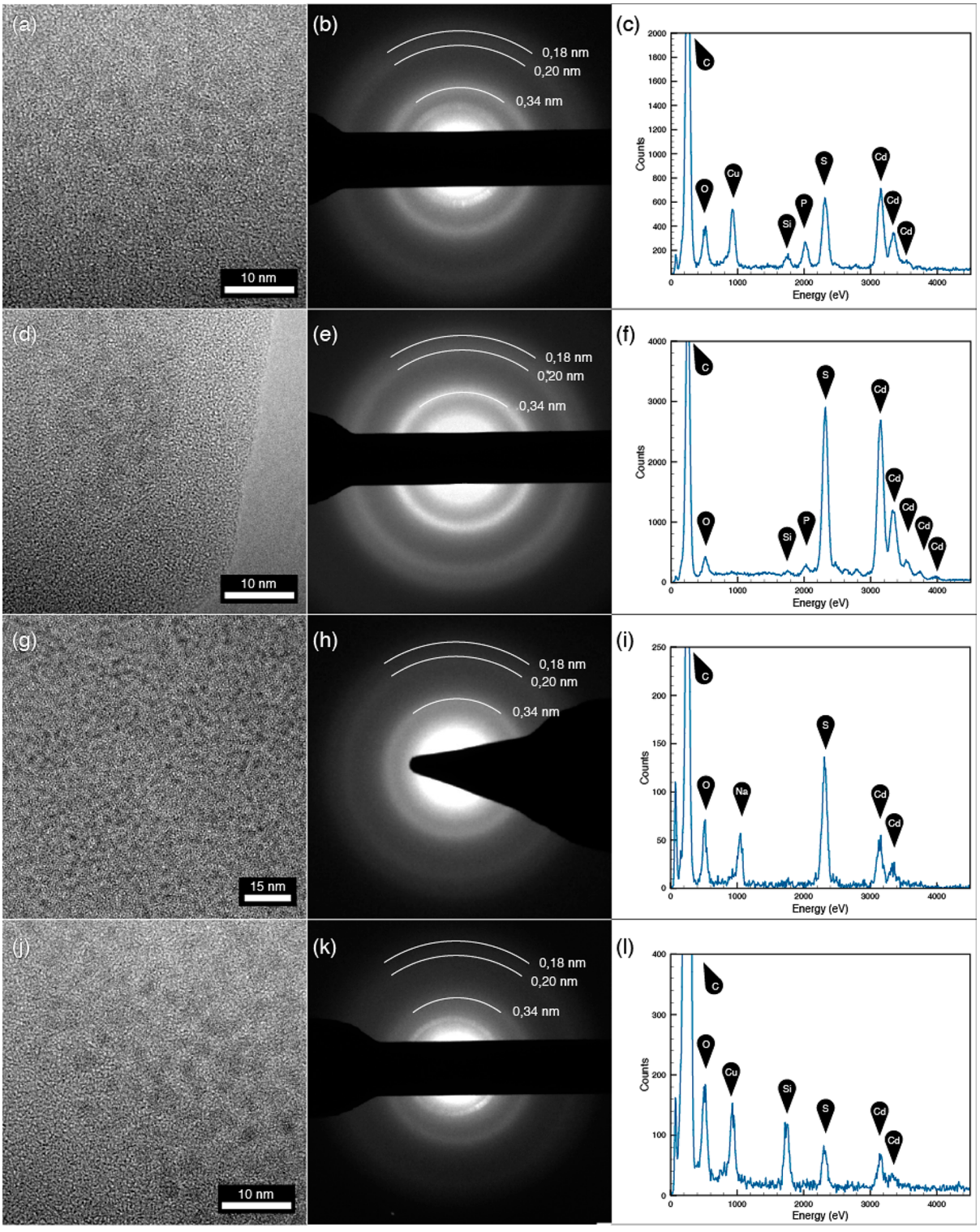

Figure 5. TEM results showing structural and compositional characterization of QDs formulations: (a–c) TOPO sample results. (a) TEM micrograph, showing QDs with darker contrast on the TEM grid. (b) Electron diffraction pattern, showing CdS cubic phase (111), (220), and (311) reflections, respectively, corresponding to interplanar distances of 0.34, 0.21, and 0.18 nm. (c) X-ray spectroscopy results of the composition of a group of QDs. Si and Cu originate from the TEM grid. (d–f) TOPO/DPP results. (g–i) Results from ODE samples. (j–l) ODE/DPP sample.

device structure contained a monolayer of QDs: ITO/PEDOT:PSS (40 nm)/PVK (35 nm)/QD (10 nm)/B3PyMPM (60 nm)/Ca (20 nm)/Al (100 nm). In set 2, instead of QDs alone, a blend of QDs with CBP in a volume ratio of (0.05:0.95) was used. In set 3, a blend of QDs with o-DBFPPO in a volume ratio of (0.05:0.95) was used, with the other layers the same as for sets 1 and 2. In all three types of devices, the EL spectrum is very similar to the PL spectrum as shown in Figure 6. It shows only emission from the QDs with a broad peak at 760 nm. It is important to note that no host emission was visible from either of the blends, implying either

DOI: 10.1021/acs.jpcc.5b09109
J. Phys. Chem. C 2016, 120, 1871–1880

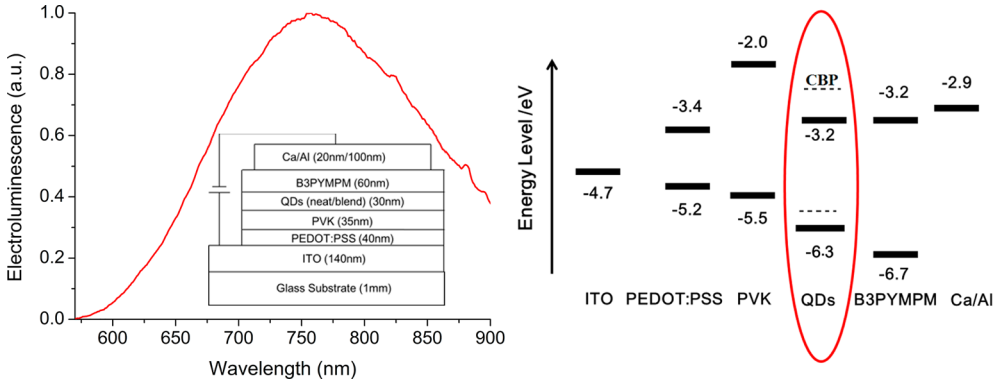

Figure 6. Diagram showing the OLED device structure and corresponding energy levels of various layers together with electroluminescence spectra.

complete energy transfer from host to the QDs or direct excitation formation on the QDs.

Figure 7a shows the external quantum efficiency of all three sets of devices. For set 1 (monolayer of QDs), the EQE is less

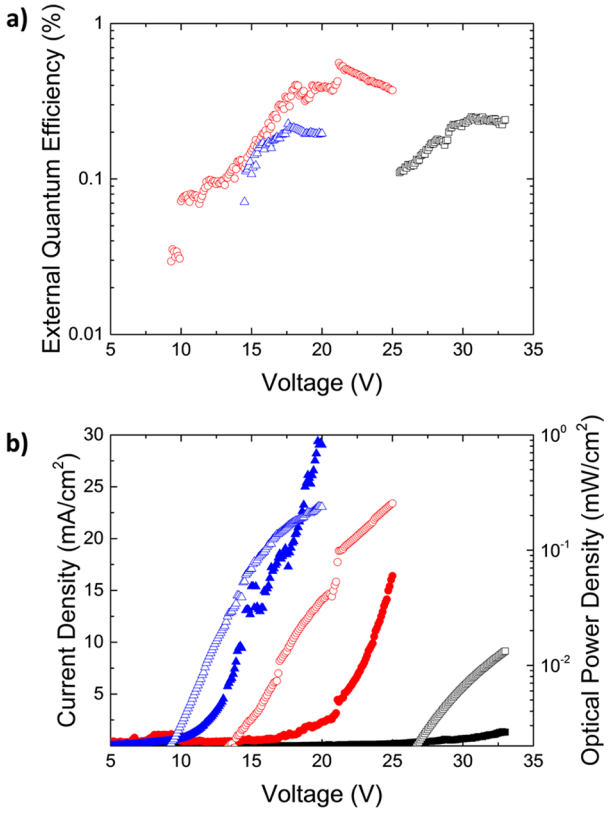

Figure 7. (a) External quantum efficiency as a function of the drive voltage. Black squares are for devices with neat quantum dots as the emissive layer (set 1). Red circles are for devices with quantum dots:CBP blend as the emissive layer (set 2). Blue triangles are for devices with quantum dots:o-DBFPPO blend as the emissive layer (set 3). (b) Current density and optical power density as a function of the driven voltage (solid dots represent the current density; hollow dots represent the optical power density).

than 0.2% in comparison to set 2 (QD:CBP blend) where EQE reaches to 0.62 ± 0.05%. In device set 3, EQE is low and less than 0.2 ± 0.02%. Figure 7b shows the current−voltage−light output characteristics for all three sets of devices. The turn on voltage for device set 1 is above 25 V, which reduces drastically in device set 2 to 15 V and in device set 3 even reduces further to just less than 10 V. The low EQE and very high turn on voltage in the case of device set 1 suggest insufficient charge transport when the excitons are directly formed in a monolayer of QDs. The energy level diagram shown in Figure 6 shows that the HOMO level of PVK is at 5.5 eV, so there is a large energy step for hole injection from this layer into the QDs which have a HOMO energy level at 6.3 eV. In contrast, there is not a barrier to electron injection. This large difference in the injection barriers for electrons and holes into the QDs results in a carrier imbalance that leads to the low efficiency of the devices made from the neat film. The carrier imbalance may also be due to quenching of excitons by the injected charge.[39] The blending of QDs with host materials improves the charge injection, as this process reduces the energy level step and can improve the efficiency. The implication of this is that excitons will not form directly on the QDs. As seen in Figure 7a, device set 2, which uses a CBP host, an ambipolar host material, improves the efficiency to 0.62 ± 0.05%. This improvement in efficiency in CBP devices is due to the reduced barrier to hole injection into the light-emitting layer as the HOMO energy of CBP is 5.95 eV, closer to that of PVK. In contrast, the efficiency does not improve in device set 3 where o-DBFPPO, an electron transport material, is used whose HOMO level (5.96 eV) is similar to CBP, although it reduces the turn on voltage substantially as shown in Figure 7b. Two factors which contribute to the higher current and lower turn-on voltage in the o-DBFPPO devices are higher electron mobility and lower barrier to electron injection as its LUMO level is 2.8 eV in comparison to the LUMO level of CBP which is 2.6 eV. Even for CBP host devices, hole injection is limited by a high-energy barrier of 0.45 eV, and the resulting charge imbalance explains why the external efficiency is much lower than might be expected for the high PLQY. These results suggest the performance of the devices can be optimized further if the charge transfer can be balanced.

4. CONCLUSIONS

In summary, we have demonstrated the use of colloidal quantum dots as efficient electroluminescent materials in organic light-emitting diodes in the biological tissue window of 700−900 nm. We have reported the highest PLQY of 34% for neat ligand-capped QDs in thin film and 69% in solutions in the near-infrared regions and achieve this using TOPO capped CdS QDs. The high PLQY coupled with a PL emission in the 700−900 nm region is due to the action of the ligands OA, TOPO, and TOP (or DPP) on the QDs surface that block the cadmium and the sulfur dangling bonds, respectively. By

DOI: 10.1021/acs.jpcc.5b09109
J. Phys. Chem. C 2016, 120, 1871−1880

utilization of a solution processable multilayer device, electroluminescence has been observed, and EL quantum efficiency up to 0.62% is achieved. Our results show that broad long wavelength emission produced by colloidal cadmium sulfide QDs can be useful to fabricate near-infrared light-emitting devices.

AUTHOR INFORMATION

Corresponding Author

*E-mail: idws@st-andrews.ac.uk.

Author Contributions

▽A.K.B. and F.A. contributed equally.

Notes

The authors declare no competing financial interest.

ACKNOWLEDGMENTS

We acknowledge financial support from FP7 project "Laser-Induced Synthesis of Polymeric Nanocomposite Materials and Development of Micro-Patterned Hybrid Light Emitting Diodes (LED) and Transistors (LET)"-LAMP (Project G. A.247928). A.K.B. and I.D.W.S. also acknowledge financial support from EPSRC Programme "Challenging the Limits of Photonics: Structured Light" Grant EP/J01771X/1. I.D.W.S. acknowledges support from a Royal Society Wolfson research merit award. The research data supporting this publication can be accessed at http://dx.doi.org/10.17630/d86a2a34-29a8-4215-a8e5-296f89943360.

REFERENCES

(1) Steigerwald, M. L.; Alivisatos, A. P.; Gibson, J. M.; Harris, T. D.; Kortan, R.; Muller, A. J.; Thayer, A. M.; Duncan, T. M.; Douglass, D. C.; Brus, L. E. Surface Derivatization and Isolation of Semiconductor Cluster Molecules. *J. Am. Chem. Soc.* **1988**, *110*, 3046−3050.

(2) Stouwdam, J. W.; Janssen, R. A. J. Red, Green, and Blue Quantum Dot LEDs with Solution Processable ZnO Nanocrystal Electron Injection Layers. *J. Mater. Chem.* **2008**, *18*, 1889−1894.

(3) Coe, S.; Woo, W.-K.; Bawendi, M.; Bulovic, V. Electroluminescence from Single Monolayers of Nanocrystals in Molecular Organic Devices. *Nature* **2002**, *420*, 800−803.

(4) Qian, L.; Zheng, Y.; Xue, J.; Holloway, P. H. Stable and Efficient Quantum-Dot Light-Emitting Diodes Based on Solution-Processed Multilayer Structures. *Nat. Photonics* **2011**, *5*, 543−548.

(5) Clifford, J. P.; Konstantatos, G.; Johnston, K. W.; Hoogland, S.; Levina, L.; Sargent, E. H. Fast, Sensitive and Spectrally Tuneable Colloidal-Quantum-Dot Photodetectors. *Nat. Nanotechnol.* **2009**, *4*, 40−44.

(6) Dayal, S.; Kopidakis, N.; Olson, D. C.; Ginley, D. S.; Rumbles, G. Photovoltaic Devices with a Low Band Gap Polymer and CdSe Nanostructures Exceeding 3% Efficiency. *Nano Lett.* **2010**, *10*, 239−242.

(7) Bruchez, M., Jr.; Moronne, M.; Gin, P.; Weiss, S.; Alivisatos, A. P. Semiconductor Nanocrystals as Fluorescent Biological Labels. *Science* **1998**, *281*, 2013−2016.

(8) Jang, E.; Jun, S.; Jang, H.; Lim, J.; Kim, B.; Kim, Y. White-Light-Emitting Diodes with Quantum Dot Color Converters for Display Backlights. *Adv. Mater.* **2010**, *22*, 3076−3080.

(9) Mashford, B. S.; Stevenson, M.; Popovic, Z.; Hamilton, C.; Zhou, Z.; Breen, C.; Steckel, J.; Bulovic, V.; Bawendi, M. High-Efficiency Quantum-Dot Light-Emitting Devices with Enhanced Charge Injection. *Nat. Photonics* **2013**, *7*, 407−412.

(10) Pietryga, J. M.; Schaller, R. D.; Werder, D.; Stewart, M. H.; Klimov, V. I.; Hollingsworth, J. A. Pushing the Band Gap Envelope: Mid-Infrared Emitting Colloidal PbSe Quantum Dots. *J. Am. Chem. Soc.* **2004**, *126*, 11752−11753.

(11) Hines, M. A.; Scholes, G. D. Colloidal PbS Nanocrystals with Size-Tunable near-Infrared Emission: Observation of Post-Synthesis Self-Narrowing of the Particle Size Distribution. *Adv. Mater.* **2003**, *15*, 1844−1849.

(12) Sommer, J. R.; Farley, R. T.; Graham, K. R.; Yang, Y.; Reynolds, J. R.; Xue, J.; Schanze, K. S. Efficient near-Infrared Polymer and Organic Light-Emitting Diodes Based on Electrophosphorescence from (Tetraphenyltetranaphtho[2,3]Porphyrin)Platinum(II). *ACS Appl. Mater. Interfaces* **2009**, *1*, 274−278.

(13) Sun, L.; Choi, J. J.; Stachnik, D.; Bartnik, A. C.; Hyun, B.-R.; Malliaras, G. G.; Hanrath, T.; Wise, F. W. Bright Infrared Quantum-Dot Light-Emitting Diodes through Inter-Dot Spacing Control. *Nat. Nanotechnol.* **2012**, *7*, 369−373.

(14) Bourdakos, K. N.; Dissanayake, D. M. N. M.; Lutz, T.; Silva, S. R. P.; Curry, R. J. Highly Efficient Near-Infrared Hybrid Organic-Inorganic Nanocrystal Electroluminescence Device. *Appl. Phys. Lett.* **2008**, *92*, 153311.

(15) Vander Heiden, M. G. Targeting Cancer Metabolism: A Therapeutic Window Opens. *Nat. Rev. Drug Discovery* **2011**, *10*, 671−684.

(16) Yu, P.; Beard, M. C.; Ellingson, R. J.; Ferrere, S.; Curtis, C.; Drexler, J.; Luiszer, F.; Nozik, A. J. Absorption Cross-Section and Related Optical Properties of Colloidal InAs Quantum Dots. *J. Phys. Chem. B* **2005**, *109*, 7084−7087.

(17) Yu, W. W.; Qu, L.; Guo, W.; Peng, X. Experimental Determination of the Extinction Coefficient of CdTe, CdSe, and CdS Nanocrystals. *Chem. Mater.* **2003**, *15*, 2854−2860.

(18) Greenham, N. C.; Samuel, I. D. W.; Hayes, G. R.; Phillips, R. T.; Kessener, Y. A. R. R.; Moratti, S. C.; Holmes, A. B.; Friend, R. H. Measurement of Absolute Photoluminescence Quantum Efficiencies in Conjugated Polymers. *Chem. Phys. Lett.* **1995**, *241*, 89−96.

(19) Rees, W. S.; Kräuter, G. Preparation and Characterization of Several Group 12 Element (Zn, Cd)-Bis(Thiolate) Complexes and Evaluation of Their Potential as Precursors for 12−16 Semiconducting Materials. *J. Mater. Res.* **1996**, *11*, 3005−3016.

(20) Talapin, D. V.; Lee, J.-S.; Kovalenko, M. V.; Shevchenko, E. V. Prospects of Colloidal Nanocrystals for Electronic and Optoelectronic Applications. *Chem. Rev.* **2010**, *110*, 389−458.

(21) Silva, F.; Carvalho, M.; Mendonca, R.; Macedo, W.; Balzuweit, K.; Reiss, P.; Schiavon, M. Effect of Surface Ligands on the Optical Properties of Aqueous Soluble CdTe Quantum Dots. *Nanoscale Res. Lett.* **2012**, *7*, 536.

(22) Wang, F.; Richards, V. N.; Shields, S. P.; Buhro, W. E. Kinetics and Mechanisms of Aggregative Nanocrystal Growth. *Chem. Mater.* **2014**, *26*, 5−21.

(23) Peng, X.; Wickham, J.; Alivisatos, A. P. Kinetics of II-VI and III-V Colloidal Semiconductor Nanocrystal Growth: "Focusing" of Size Distributions. *J. Am. Chem. Soc.* **1998**, *120*, 5343−5344.

(24) Wei, H. H.-Y.; Evans, C. M.; Swartz, B. D.; Neukirch, A. J.; Young, J.; Prezhdo, O. V.; Krauss, T. D. Colloidal Semiconductor Quantum Dots with Tunable Surface Composition. *Nano Lett.* **2012**, *12*, 4465−4471.

(25) Anderson, N. C.; Hendricks, M. P.; Choi, J. J.; Owen, J. S. Ligand Exchange and the Stoichiometry of Metal Chalcogenide Nanocrystals: Spectroscopic Observation of Facile Metal-Carboxylate Displacement and Binding. *J. Am. Chem. Soc.* **2013**, *135*, 18536−18548.

(26) Leubner, S.; Schneider, R.; Dubavik, A.; Hatami, S.; Gaponik, N.; Resch-Genger, U.; Eychmuller, A. Influence of the Stabilizing Ligand on the Quality, Signal-Relevant Optical Properties and Stability of near-Infrared Emitting $Cd_{1-x}Hg_xTe$ Nanocrystals. *J. Mater. Chem. C* **2014**, *2*, 5011−5018.

(27) Rogach, A. L.; Franzl, T.; Klar, T. A.; Feldmann, J.; Gaponik, N.; Lesnyak, V.; Shavel, A.; Eychmüller, A.; Rakovich, Y. P.; Donegan, J. F. Aqueous Synthesis of Thiol-Capped CdTe Nanocrystals: State-of-the-Art. *J. Phys. Chem. C* **2007**, *111*, 14628−14637.

(28) Dolai, S.; Nimmala, P. R.; Mandal, M.; Muhoberac, B. B.; Dria, K.; Dass, A.; Sardar, R. Isolation of Bright Blue Light-Emitting CdSe Nanocrystals with 6.5 KDa Core in Gram Scale: High Photo-

DOI: 10.1021/acs.jpcc.5b09109
J. Phys. Chem. C 2016, 120, 1871−1880

luminescence Efficiency Controlled by Surface Ligand Chemistry. *Chem. Mater.* **2014**, *26*, 1278−1285.
(29) Subila, K. B.; Kishore Kumar, G.; Shivaprasad, S. M.; George Thomas, K. Luminescence Properties of CdSe Quantum Dots: Role of Crystal Structure and Surface Composition. *J. Phys. Chem. Lett.* **2013**, *4*, 2774−2779.
(30) Bullen, C.; Mulvaney, P. The Effects of Chemisorption on the Luminescence of CdSe Quantum Dots. *Langmuir* **2006**, *22*, 3007−3013.
(31) Wang, F.; Buhro, W. E. Morphology Control of Cadmium Selenide Nanocrystals: Insights into the Roles of Di-N-Octylphosphine Oxide (DOPO) and Di-N-Octylphosphinic Acid (DOPA). *J. Am. Chem. Soc.* **2012**, *134*, 5369−5380.
(32) Wang, F.; Tang, R.; Buhro, W. E. The Trouble with TOPO; Identification of Adventitious Impurities Beneficial to the Growth of Cadmium Selenide Quantum Dots, Rods, and Wires. *Nano Lett.* **2008**, *8*, 3521−3524.
(33) Yu, K.; Liu, X.; Zeng, Q.; Leek, D. M.; Ouyang, J.; Whitmore, K. M.; Ripmeester, J. A.; Tao, Y.; Yang, M. Effect of Tertiary and Secondary Phosphines on Low-Temperature Formation of Quantum Dots. *Angew. Chem., Int. Ed.* **2013**, *52*, 4823−4828.
(34) Williams, E. S.; Major, K. J.; Tobias, A.; Woodall, D.; Morales, V.; Lippincott, C.; Moyer, P. J.; Jones, M. Characterizing the Influence of TOPO on Exciton Recombination Dynamics in Colloidal CdSe Quantum Dots. *J. Phys. Chem. C* **2013**, *117*, 4227−4237.
(35) Sines, I. T.; Schaak, R. E. Phase-Selective Chemical Extraction of Selenium and Sulfur from Nanoscale Metal Chalcogenides: A General Strategy for Synthesis, Purification, and Phase Targeting. *J. Am. Chem. Soc.* **2011**, *133*, 1294−1297.
(36) Haram, S. K.; Quinn, B. M.; Bard, A. J. Electrochemistry of CdSe Nanoparticles: A Correlation between Optical and Electrochemical Band Gaps. *J. Am. Chem. Soc.* **2001**, *123*, 8860−8861.
(37) Han, C.; Xie, G.; Xu, H.; Zhang, Z.; Yu, D.; Zhao, Y.; Yan, P.; Deng, Z.; Li, Q.; Liu, S. Towards Highly Efficient Blue-Phosphorescent Organic Light-Emitting Diodes with Low Operating Voltage and Excellent Efficiency Stability. *Chem. - Eur. J.* **2011**, *17*, 445−449.
(38) Tanaka, D.; Sasabe, H.; Li, Y.-J.; Su, S.-J.; Takeda, T.; Kido, J. Ultra High Efficiency Green Organic Light-Emitting Devices. *Jpn. J. Appl. Phys.* **2007**, *46*, L10−12.
(39) Kobayashi, Y.; Nishimura, T.; Yamaguchi, H.; Tamai, N. Effect of Surface Defects on Auger Recombination in Colloidal CdS Quantum Dots. *J. Phys. Chem. Lett.* **2011**, *2*, 1051−1055.

DOI: 10.1021/acs.jpcc.5b09109
J. Phys. Chem. C 2016, 120, 1871−1880